Fast Numerical simulations of 2D turbulence using a dynamic model for Subgrid Motions

J-P. Laval[1], B. Dubrulle[2,3] and S. V. Nazarenko[4]

December 12, 2001

[1] CEA/DAPNIA/SAp, CE Saclay, 91191 Gif sur Yvette Cedex, France

[2] NCAR, P.O. Box 3000, Boulder CO 80307-3000

[3] CNRS, URA 285, Observatoire Midi-Pyrénées, 14 avenue Belin, F-31400 Toulouse, France

[4] Mathematics Institute University of Warwick COVENTRY CV4 7AL, UK

Abstract

We present numerical simulation of 2D turbulent flow using a new model for the subgrid scales which are computed using a dynamic equation linking the subgrid scales with the resolved velocity. This equation is not postulated, but derived from the constitutive equations under the assumption that the non-linear interactions of subgrid scales between themselves are equivalent to a turbulent viscosity. This results in a linear stochastic equation for the subgrid scales, which can be numerically solved by a decomposition of the subgrid scales into localized wave-packets. These wave-packets are transported by the resolved scale velocity and have wavenumbers and amplitude which evolve according to the resolved strain and the stochastic forcing. The performances of our model are compared with Direct Numerical Simulations of decaying and forced turbulence. For a same resolution, numerical simulations using our model allow for a significant reduction of the computational time (of the order of 100 in the case we consider), and allow the achievement of significantly larger Reynolds number than the direct method.

1 Introduction

The dynamics of high Reynolds number turbulent flow couples a large range of scales from the characteristic size of the domain to the dissipative scales. This range is usually too large to be fully resolved by Direct Numerical Simulation of the Navier-Stokes equations (DNS). This is the case for many applications like in aeronautics, geophysics or astrophysics where the typical Reynolds numbers are of the order of 10^6 to 10^{12}. The largest Reynolds numbers which can be achieved by DNS are of the order of 10^4 to 10^5 [1, 2]. The difficulty of direct simulation of turbulent flows at high Reynolds number arises because of two scaling laws: first, the memory requirement to be able to deal with all the scale of motions growths like $Re^{9/4}$, where Re is the Reynolds number; second, the time stepping to be used to advance the equations has to be computed using the smallest resolved scale. As a result, computational time usually growths like Re^3. Despite of the growth of the computer power [3], the direct simulation of all realistic problems will not be conceivable before a long time.

Part of these difficulties could be circumvented if one could find an efficient approximate scheme to model the small scales of the turbulent flow, which usually monopolize 90 per cent of the computations and, for most applications, do not need to be known with the same precision as the large scales. From an algorithmic point of view, several methods have been proposed to try to describe the small turbulent scales with less degree of freedom than in a DNS like for example, sparse Fourier transform [4], rarefied modes [5], wavelets [6], self-adaptative grid mesh [7, 8]. From a theoretical point of view, the effort has been put on the model of the action of the small scales onto the larger scales of motion, or onto the small scales themselves, to be able to deal with simpler and cheaper systems to compute. In the extreme case of large eddy simulations (LES) or random averaged numerical simulations (RANS), the effect of the small scales at large scales is directly modeled as a function of the resolved or mean scales of motions, resulting in both memory and computational gain. This is often done at the price of introduction of arbitrary parameters, which require calibration and which lower the predictive power of the simulation. Also, some models are not theoretically satisfying, since they break for example the basic symmetries of the original equations [9].

In this paper, we continue a study initiated in [10] and develop a new dynamic model for the turbulent subgrid quantities which is directly derived from the constitutive equations of motions. This model respects all

the basic symmetries of the original equations, as well as their conservation properties. The main assumption underlying the model is that the smaller turbulent scales are much less energetic than the resolved scales, and so, that their main interactions are with the resolved flow. It then appears reasonable to try to model these main interactions with as few approximations as possible, while more freedom is allowed regarding their mutual interactions. In the model we consider, the interactions between the resolved and subgrid scales are taken into account without any approximation, while the mutual interactions between subgrid scales are replaced by a turbulent viscosity. In 2D geometry, where energy condensation at large scale guarantees that the dynamics of the small scales is mainly non-local in scales this turbulent viscosity is so small that it can be set to zero in some simple cases [11]. This allows a parameter free model of the subgrid scales, which will be described in the first part of this paper. In situations where dynamic processes at small scales, like vortex stretching, are important to regulate any small-scale instability, or even in 2D when "large" and "small" scales are not well enough separated, the turbulent viscosity cannot be set to zero [12]. This option introduces a free parameter into the model, but, since it appears at a sub-dominant level, we may expect that its choice is not so critical to the success of the model.

After parameterization of the non-linear interactions between the subgrid scales, their resulting equation of motion becomes linear. This essential feature has two advantages: first, it enables, in certain simple flow geometries, analytical solutions for the subgrid-scale dynamics as a function of the resolved quantities, thereby closing the equations of motions at the resolved-scale level. This property was used to obtain analytical solution for mean profiles in channel flows [13, 14, 15] or for the Planetary Surface Layer [16, 17]. Second advantage of the linear description is that it allows for more efficient algorithms of integrations, using Lagrangian methods where the time stepping is done via a criterion based on the resolved scales. This allows numerical computations with a larger time step than DNS, and thus, at a lower computational cost.

An essential part of our model is the averaged Reynolds stresses describing the feedback of the subgrid scales onto the resolved component. In [10], we considered the scale separation parameter to be much less than the nonlinearity of the small scales and derived a feedback term in which the quadratic in the small-scale amplitude terms gave the main contribution into the Reynolds stress. Then, the model that consisted of two coupled "fluids" (the resolved and the subgrid one) was used to solve several problems

with ([18]) and without scale separation ([10]), the later being the typical problems such as the forced turbulence, the vortex merger and a turbulence decay. It was noticed that in the problems without a natural scale separation, such a model described very well the small-scale dynamics whereas improvements in modeling of the large scales (which is the main aim of the LES) was much more modest. The situation was clarified in [11] where direct numerical evaluations of the different contributions to the Reynolds stress were made. It was shown that in the problems without the scale separation the dominant contribution to the Reynolds stress comes from the linear rather than quadratic in the small-scale amplitude term.

In the present contribution, we focus on advancing the numerical approach introduced in [10] by introducing a better model for the turbulent Reynolds stress based on the results of the a priori tests performed in [11]. Also, a more efficient procedure is used in this paper to generate the subgrid vorticity and velocity fields. Our goal here is to test our model both as a numerical method for an improved DNS, in the sense that we can compute the whole range of scales at a lower computational cost, and as pseudo LES method, in the sense that we compute only the larger scales, at an even lower computational cost. For the sake of simplicity, we shall consider here only the two-dimensional case, where both the hypothesis of the turbulent model [11] and its consequences [18, 10] have been studied in detail. The generalization to the 3D case is the subject of an ongoing research.

2 The turbulence model

2.1 Scale decomposition

We consider a two-dimensional incompressible inviscid flow obeying the equations:

$$\left\{ \begin{array}{lcl} \partial_t \omega + \mathrm{div}(\mathbf{u}\omega) & = & \nu \Delta \omega, \\ \mathrm{div}\, \mathbf{u} & = & 0, \end{array} \right. \tag{1}$$

where $\mathbf{u}$ is the velocity and ν is the viscosity. In 2D geometry, the vorticity has only one non-zero component that we denote by ω. The resolved- and the subgrid-scale part of the velocity and the vorticity fields are defined via a filtering procedure:

$$\mathbf{U}(\mathbf{x},t) \;=\; \overline{\mathbf{u}(\mathbf{x},t)} = \int G(\mathbf{x}-\mathbf{x}')\mathbf{u}(\mathbf{x}',t)d\mathbf{x}' \tag{2}$$

$$\Omega(\mathbf{x},t) \;=\; \overline{\omega(\mathbf{x},t)} = \int G(\mathbf{x}-\mathbf{x}')\omega(\mathbf{x}',t)d\mathbf{x}' \tag{3}$$

Here, G is a filter, such that the resolved scales contain the main part of the total energy. In Section III.C, we shall propose a special shape of G obeying this condition, and which is well adapted to our numerical method.

Each field is then decomposed as follows

$$\mathbf{u}(\mathbf{x},t) \;=\; \mathbf{U}(\mathbf{x},t) + \mathbf{u}'(\mathbf{x},t), \tag{4}$$
$$\omega(\mathbf{x},t) \;=\; \Omega(\mathbf{x},t) + \omega'(\mathbf{x},t), \tag{5}$$

where the primes denote subgrid-scale quantities. Inserting this decomposition into the Navier-Stokes equations and separating the resolved and the subgrid-scale parts, we get a set of coupled equations:

$$\begin{aligned}\partial_t\Omega \;&+\; \mathrm{div}\,(\overline{\mathbf{U}\Omega}) + \mathrm{div}\,(\overline{\mathbf{u}'\Omega}) \\ &+\; \mathrm{div}\,(\overline{\mathbf{U}\omega'}) + \mathrm{div}\,(\overline{\mathbf{u}'\omega'}) = \nu\Delta\Omega,\end{aligned} \tag{6}$$

and

$$\begin{aligned}\partial_t\omega' \;&+\; \mathrm{div}\,(\mathbf{U}\Omega) - \mathrm{div}\,(\overline{\mathbf{U}\Omega}) \\ &+\; \mathrm{div}\,(\mathbf{U}\omega') - \mathrm{div}\,(\overline{\mathbf{U}\omega'}) \\ &+\; \mathrm{div}\,(u'\Omega) - \mathrm{div}\,(\overline{u'\Omega}) \\ &+\; \mathrm{div}\,(u'\omega') - \mathrm{div}\,(\overline{u'\omega'}) = \nu\Delta\omega'.\end{aligned} \tag{7}$$

The second up to the sixth terms of the l.h.s. of (7) are the contributions due to non-local interactions between the resolved and the subgrid scales. The last two terms in the l.h.s. of (7) are the contributions due to non-linear (local in scale space) interactions among the subgrid scales. In the favorable case where most of the energy is at the resolved scales, these last two terms can be expected to negligible with respect to, e.g., the second up to the fourth terms of the l.h.s. of (7). Indeed, in a recent detailed numerical analysis of the system (6) and (7), Laval et al [11] showed that for a very steep filter (when the filter G is a cut-off in the spectral space), the small-scale dynamics (and thus the large-scale dynamics) is independent of the local interactions: when the later are neglected, the small-scale velocity and vorticity field are not significantly changed, in both forced and decaying turbulence, even after several eddy turn-over times [11]. The analysis has also shown that in 2D turbulence, the leading order contribution at both large and small-scale comes from the correlations involving the large-scale

velocity field, i.e. $\mathbf{U}\Omega$ and $\mathbf{U}\omega'$. The next leading order contribution comes from the correlations between small-scale velocity and vorticity $u'\omega'$, while the correlation between small-scale velocity and large-scale vorticity $u'\Omega$ gives the lowest contribution.

2.2 A priori numerical estimates

In the present case, the filter G is smoother, and subgrid scales include both large and small scales. It is thus important to conduct additional numerical evaluation of the various terms of (6) and (7) using a smooth filter, to check the validity of the non-locality assumption for the subgrid scales. We performed an apriori test with the filter which will be used in our model. The choice of the filter will be discussed in section D. The test was done using a vorticity field from a DNS on a 1024^2 grid. The Figures 1 and 2 give the distribution of each non-linear terms involved in the resolved scales and the subfilter-scales equations. The result of the filtering process one the initial field is shown fig. 3. Even with a smooth filter, the non-linear term involving only subgrid scales are still small compared to the higher order term.

2.3 The model

Keeping only the leading order contributions, the coupled equations (6) and (7) become:

$$\partial_t \Omega + \operatorname{div} \overline{\mathbf{U}\Omega} + \operatorname{div} \overline{\mathbf{U}\omega'} = \nu \Delta \Omega, \tag{8}$$

$$\begin{aligned} \partial_t \omega' + \operatorname{div} (\mathbf{U}\omega') &= F + \nu_t \Delta \omega', \\ F(\mathbf{x}, t) &= -(\operatorname{div} (\mathbf{U}\Omega) - \operatorname{div} \overline{\mathbf{U}\Omega}) + \operatorname{div} \overline{\mathbf{U}\omega'}. \end{aligned} \tag{9}$$

Here, ν_t is a turbulent viscosity, which will be introduced to damp the small-scale noise arising in our numerical scheme and F is a force which describes the subgrid-scale generation via the enstrophy cascade (energy cascade in 3D).

3 Numerical implementation

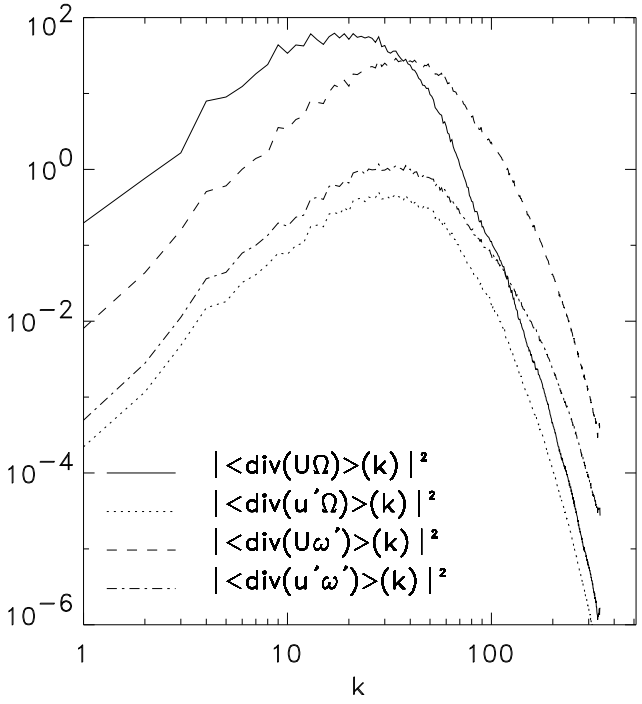

Figure 1: Comparison of the square moduli of each component of the nonlinear part of the large scale equation 6 in Fourier space. The filter used for the scale separation is a smooth filter in Fourier space defined by eq. (23). The energy spectra of both resolved scales and subfilter scales are shown fig. 3

3.1 Numerical strategy and performances

The resolved-scale equation has the form of an Euler equation with an additional forcing coming from the interaction with the subgrid-scale motions. One is therefore led to standard strategies to solve this equation, depending on the type of the flow (spectral methods for flows in simple periodic geometry, or finite difference or finite elements for more complicated geometries). Here, we shall consider the periodic case, thereby using a spectral code for solving the resolved-scale equation. This code is described in [19].

The situation is markedly different at the subgrid level, where the basic equation is *linear* in the subgrid motions, with an inhomogeneous part

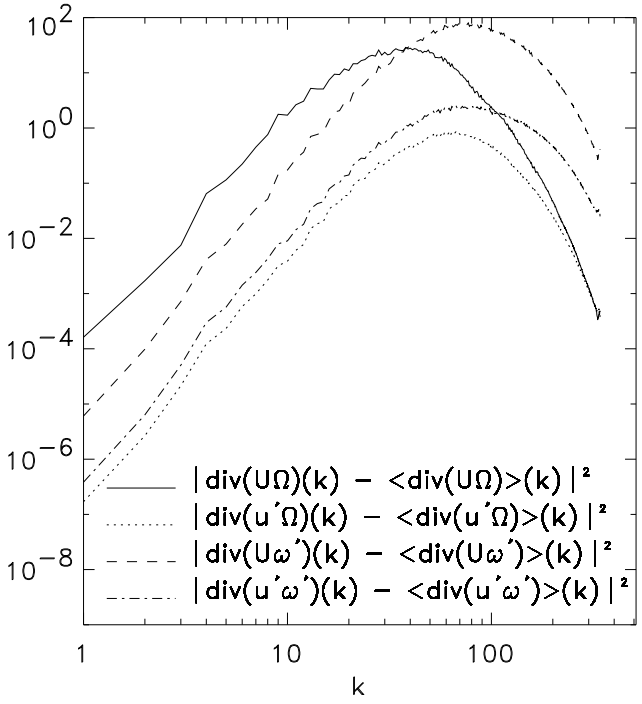

Figure 2: Same comparison as in fig. 1 but now for the non-linear terms in the subfilter scale equation.

provided by the subgrid scale generation via the enstrophy cascade. This linearity suggests a solution strategy based on projection of the subgrid scales onto appropriate modes. Since the subgrid scales are usually very inhomogeneous (e.g., vorticity filaments), it seems logical to use a decomposition of the subgrid-scale velocity field into localized modes, thereby optimizing the memory requirements to store the subgrid-scale fields. A popular local mode decomposition uses wavelets (see e.g. [20]). Wavelets are however sometimes difficult to implement, and are not very handy to use in analytical computations. Here, we choose to use a Gabor decomposition, which provides a localized description while allowing theoretical manipulations similar to that obtained with Fourier modes. The linearity of the subgrid motions also provides room for a further computational time reduction via semi-Lagrangian methods of integration, using a time step related to the resolved scale. The

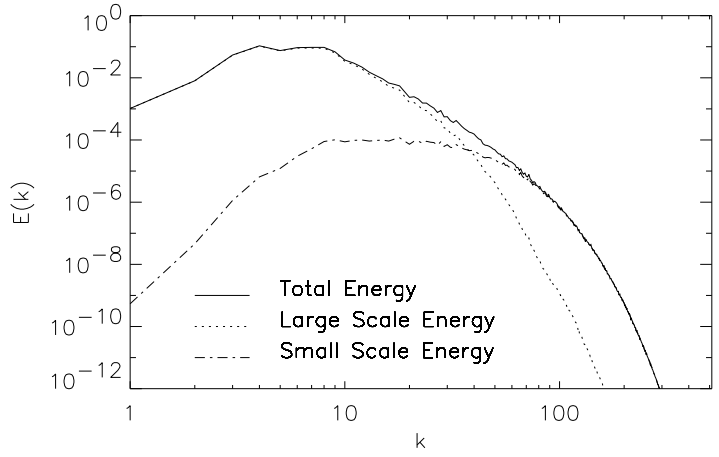

Figure 3: Energy spectra of the resolved and the subfilter components for the same run as in fig. 1 and 2. The filter used for the scale separation is defined in eq. (23) with $dh = 2\pi/32$. The initial field is the result of a Direct Numerical Simulation of decaying turbulence on a 1024^2 grid.

numerical expected performances of our model, integrated using the semi-Lagrangian, Gabor method, at a given resolution and total integration time, is given in Table 1, and compared with both standard spectral methods based on FFT, and a LES approach based on FFT. Computational time for several particular examples is given in table 2 which shows an obvious gain in speed for our method with respect to the DNS. If we now compare with a classical LES, our method is somewhat slower because it is necessary to keep a sufficient number of localized modes for accurate description of the Reynolds stresses. However, a substantial gain in accuracy is achieved in comparison with traditional LES because of the better description of the nonlocal interaction of scales.

3.2 Description of the algorithm

Our algorithm of resolution of the turbulent model is based on five steps:

1 Compute the force F (9) using the resolved and subgrid fields at time t;

2 Project this force onto a set of Gabor modes;

Model (resolution)	integration time
DNS [FFT code] (N x N)	$c_1 * N^2 log(N)$
LES [FFT code] (M x M)	$c_2 * M^2 log(M)$
Our Model [FFT + Lagr.]	$c_3 * M^2 log(M) + c_4 * N_p$

Table 1: Comparison of expected performance between DNS, Classical LES models (like APVM or HDNS) based on FFT on a (M x M) grid and our model on a (M x M) grid for fully resolved scales and N_p modes for approximated subfilter scale equation (see section 3.5).

Model	$\tau = 15$	$\tau = 50$	Comp. time
DNS ($N = 1024$)	——	——	$\sim$ 10 days
M0 ($M = 64, N_p = 512^2$)	0.99403	0.89794	$\sim$ 1h30
M1 ($M = 64, N_p = 512^2$)	0.99450	0.82523	$\sim$ 1h30
M2 ($M = 64, N_p = 128^2$)	0.99409	0.89735	$\sim$ 8 mn
APVM ($M = 64^2$)	0.95882	0.77429	$\sim$ 2 mn
HDNS ($M = 64^2$)	0.93893	0.53231	$\sim$ 2 mn

Table 2: Correlation between large-scale ($k < 21$) vorticity from DNS and vorticity field from : our model with a maximum of 512^2 particles (M0 and M1) and 128^2 particles (M2), the APVM model and an hyper-viscous simulation both on the resolved-scale grid $N = 64^2$. The same viscosity as in DNS was introduced in the resolved scale equation for the M1 simulation whereas no viscosity was introduced for the M0 and M2 simulations. The correlation coefficient are given at two different times (15 and 50 turnover times). The computations time with a "Sun Ultrasparc 3000 workstation" are given in the last column.

3 Advance the subgrid field to time $t + dt$ in the Gabor space using this projection and the Lagrangian advection algorithm;

4 Compute the resolved Reynolds stresses at time $t+dt$ using a procedure similar to an inverse Gabor transform;

5 Advance the resolved velocity field at time $t + dt$ using this Reynolds stress.

Step 1 and 5 involve standard procedures linked with our resolved scale code (in the present case a Fourier spectral code with an Adams-Bashforth time stepping where a full desaliasing was introduced by keeping only the first 2/3 smaller wavenumbers in each direction, see [19]). Step 2, 3 and 4 involve new original procedures, based on interesting properties of the Gabor transform. For the sake of clarity , we present here only main results, leaving detailed computations in appendices.

3.3 The continuous Gabor transform

The Gabor transform (GT) is defined as

$$\hat{\mathbf{u}'}(\mathbf{x}, \mathbf{k}, t) \;=\; \int f(\epsilon^*(\mathbf{x} - \mathbf{x}'))\, e^{i\mathbf{k}\cdot(\mathbf{x}-\mathbf{x}')}\, \mathbf{u}'(\mathbf{x}')\, d\mathbf{x}', \tag{10}$$

where f is a rapidly decreasing function at infinity. Note that $1/\epsilon^*$ has a meaning of the scale separation length. It has to be chosen to lie in between of the integral scale and the Kolmogorov scale, the later being far in the subgrid range in many applications. For LES purposes, $1/\epsilon^*$ has to be close to (but not less than) the minimal resolved scale (grid scale dh in our case). Thus, to derive our model we need to assume the subfilter-scale wavenumber k to be greater than ϵ^* and use ϵ^*/k as a small parameter. Technically, however, is convinient to keep k fixed and perform expansions in small ϵ^*.

In the special case where $f = \sqrt{G}$, where G is the filter (see eq. (3)), we have the following simple reconstruction formulae:

$$\mathbf{u}'(\mathbf{x}, t) = \frac{1}{(2\pi)^2\, f(0)} \int \hat{\mathbf{u}'}(\mathbf{x}, \mathbf{k}, t) d\mathbf{k}, \tag{11}$$

$$\overline{\mathbf{U}\omega'}(\mathbf{x}, t) = \mathbf{U}\frac{1}{(2\pi)^2} \int \Re\left[\hat{\omega'}(\mathbf{x}, \mathbf{k}, t) f(-\mathbf{k}, t)\right] d\mathbf{k} + O(\epsilon^*), \tag{12}$$

where $\Re$ means the real part, and finally

$$\overline{u_i' u_j'}(\mathbf{x}, t) = \frac{1}{(2\pi)^2} \int \Re \left[\hat{u_i'}(\mathbf{x}, \mathbf{k}, t) \hat{u_j'}(\mathbf{x}, -\mathbf{k}, t) \right] d\mathbf{k} + O(\epsilon^*). \tag{13}$$

One may also note the connection between the Gabor velocity and the Gabor vorticity (similar to the Fourier quantities):

$$\hat{\mathbf{u}}(\mathbf{k}, t) = -\frac{i}{k^2} \hat{\omega}(\mathbf{k}, t)(e_z \times \mathbf{k}) + O(\epsilon^*), \tag{14}$$

where e_z is a unit vector in z-direction.

Finally, one may show that the GT of the subgrid-scale equation (9) is (see appendix A and [13, 15] for more details)

$$\left(\partial_t + \mathbf{U} \cdot \nabla_x - \nabla_x \left(\mathbf{U} \cdot \mathbf{k}\right) \cdot \nabla_k\right) \hat{\omega'}(\mathbf{x}, \mathbf{k}, t) = \hat{F}(\mathbf{x}, t) - \nu_t k^2 \omega'(\mathbf{x}, \mathbf{k}, t). \tag{15}$$

3.4 The discretized optimum Gabor transform

The continuous Gabor transform is not suitable for numerical implementation. Moreover, because it involves both position and wavenumbers, it theoretically describes a given field via a much larger mode numbers than in traditional spectral methods (typically N^{2D} versus N^D in D dimensions). However, as discussed previously, inhomogeneous fields may be represented with a high precision by a much smaller set of Gabor modes than the theoretical number, a number even potentially smaller than N^D (see e.g. [21]). The algorithm we devised uses N^D Gabor modes and, therefore, there is a room for further code optimization.

3.4.1 The discretization

The discretization of the subgrid field in the Gabor space is done via a Particle In Cell (PIC) method. This method is traditionally used in plasma physics, but was used previously in hydrodynamics by Nazarenko *et al* [22] to study the interaction of sound wave-packets with turbulence. Details about the method can also be found in [10]. In this method, the Gabor modes of the subgrid-scale vorticity field are replaced with discrete wave-packets (particles). For example, the vorticity field $\hat{\omega'}(\mathbf{x}, \mathbf{k}, t)$ is discretized with N_p wave-packets α in the Gabor space:

$$\hat{\omega'}(\mathbf{x}, \mathbf{k}, t) = \sum_{\alpha=1}^{N_p} \hat{\sigma}_\alpha(t)\ S_{\mathbf{x}}(\mathbf{x} - \mathbf{x}_\alpha(t))\ S_{\mathbf{k}}(\mathbf{k} - \mathbf{k}_\alpha(t)). \tag{16}$$

In (16), α labels the wave-packet. Note that our representation allows several wave-packets with different wavenumbers to be located at the same position $\mathbf{x}$, like in the Gabor transform. Here $S_{\mathbf{x}}$ and $S_{\mathbf{k}}$ are some interpolating functions (particle "size"). Since the computation of non-linear terms in the resolved-scale equation involves a second order spatial derivative, we are led to choose a linear interpolation in the $\mathbf{x}$ direction. In the $\mathbf{k}$ direction, a zero particle "thickness" turns out to be sufficient for our purpose. We thus adopt the following representation,

$$S_{\mathbf{x}}(\mathbf{x}) = S(x)S(y), \tag{17}$$

$$S_{\mathbf{k}}(\mathbf{k}) = \delta(p)\delta(q), \tag{18}$$

where $\mathbf{x} = (x, y)$, $\mathbf{k} = (p, q)$, δ is the Dirac function and the function $S(\eta)$ is defined by:

$$S(\eta) = \begin{cases} (dh - |\eta|)/dh & \text{if } |\eta| < dh, \\ 0 & \text{otherwise,} \end{cases} \tag{19}$$

$$\tag{20}$$

Here, dh is a length scale governing the accuracy of the discretization. Its choice will be discussed later on.

The PIC algorithm of reconstruction of the continuous fields from the discretized coefficients provides a natural filter G and the function f to be used in the Gabor transform through (see appendix D):

$$G(\mathbf{x}) = f^2(\mathbf{x}) = f^2(0) \times S^2_{\mathbf{x}}(\mathbf{x}), \tag{21}$$

with

$$f(0) = \frac{1}{\sqrt{\int S^2_{\mathbf{x}}(\mathbf{x}')d\mathbf{x}'}}. \tag{22}$$

In the $\mathbf{k}$ space, the filtering operation is achieved by simply multiplication of the Fourier coefficients by the Fourier transform of G, which is

$$\hat{G}(p, q) = \frac{36}{(p\ dh)^2(q\ dh)^2} \left\{ \left(1 - \frac{sin(p\ dh)}{p\ dh}\right) \left(1 - \frac{sin(q\ dh)}{q\ dh}\right) \right\} \tag{23}$$

3.4.2 Reconstruction of the subgrid scale correlations

With our discretization, the formulae of reconstruction of the subgrid correlations (12) can be obtained using (16). Taking into account the condition that ω' is real, we have (see appendix C for details):

$$\overline{\mathbf{U}\omega'}(\mathbf{x},t) \simeq 2\mathbf{U} \sum_{\alpha_+=1}^{N_p} \Re\left[\hat{\sigma_{\alpha_+}} f^*(\mathbf{k}_{\alpha_+})\right] S_{\mathbf{x}}(\mathbf{x}-\mathbf{x}_{\alpha_+}), \tag{24}$$

where the sum is only over the wave-packets with positive wavenumber p_α[1]. Similarly, one can use (45) and (16) to re-write (13) as (63) (see appendix C)

$$\begin{aligned}
\overline{u'v'}(\mathbf{x},t) &= 2\sum_{\alpha_+=1}^{N_p} \frac{-q_{\alpha_+}p_{\alpha_+}}{({p_{\alpha_+}}^2+{q_{\alpha_+}}^2)^2}|\hat{\sigma}_{\alpha_+}|^2 S_{\mathbf{x}}^2(\mathbf{x}-\mathbf{x}_{\alpha_+}) \\
\overline{u'^2}(\mathbf{x},t) &= 2\sum_{\alpha_+=1}^{N_p} \frac{+q_{\alpha_+}^2}{({p_{\alpha_+}}^2+{q_{\alpha_+}}^2)^2}|\hat{\sigma}_{\alpha_+}|^2 S_{\mathbf{x}}^2(\mathbf{x}-\mathbf{x}_{\alpha_+}) \\
\overline{v'^2}(\mathbf{x},t) &= 2\sum_{\alpha_+=1}^{N_p} \frac{+p_{\alpha_+}^2}{({p_{\alpha_+}}^2+{q_{\alpha_+}}^2)^2}|\hat{\sigma}_{\alpha_+}|^2 S_{\mathbf{x}}^2(\mathbf{x}-\mathbf{x}_{\alpha_+})
\end{aligned} \tag{25}$$

3.4.3 Optimum discrete Gabor transform

For a given field $\omega'(\mathbf{x},t)$, associated with a grid of size $2\pi/N$, our "optimum" discrete Gabor transform only retains one wavenumber per position (i.e. N^2 Gabor modes, for a N^2 initial discrete field). This wavenumber, and the amplitude of the corresponding Gabor mode are chosen as follows: we use the exact relation between the field and its N^2 wave-packet components

$$\omega'(\mathbf{x},t) = \frac{2}{f(0)} \sum_{\alpha_+=1}^{N_p} \Re\left[\sigma_{\alpha_+}(t)\right] S_{\mathbf{x}}(\mathbf{x}-\mathbf{x}_\alpha). \tag{26}$$

An easy way to satisfy (26) exactly is to create one wave-packet at each grid point, so that $N_p = N^2$. Applying equation (26) at each grid point $\mathbf{x}_i$ we then obtain:

[1]. Since the vorticity $\omega'(\mathbf{x},t)$ is real, each wave-packet at position $\mathbf{x}_\alpha$ and with wavenumber $\mathbf{k}_\alpha$ will have a partner wave-packet with same amplitude, at the same location and with an opposite wavenumber $-\mathbf{k}_\alpha$.

$$\omega'(\mathbf{x}_i,t) = \frac{2}{f(0)}\Re\left[\sigma_{\alpha_i}(t)\right]. \tag{27}$$

This equation fixes the real part and the physical coordinates of the wave-packet. To find its wavenumber, we use the velocity at the grid point $u'(\mathbf{x}_i)$ to find two conditions:

$$u'(\mathbf{x}_i,t) = \frac{2}{f(0)}\frac{-q_{\alpha_i}}{(p_{\alpha_i}^2+q_{\alpha_i}^2)}\Im\left[\sigma_{\alpha_i}(t)\right], \tag{28}$$

$$v'(\mathbf{x}_i,t) = \frac{2}{f(0)}\frac{+p_{\alpha_i}}{(p_{\alpha_i}^2+q_{\alpha_i}^2)}\Im\left[\sigma_{\alpha_i}(t)\right]. \tag{29}$$

These conditions link the two components of the wavenumber with the imaginary part of the amplitude of the wave-packet, which is still a free parameter at this stage. We then select the phase of the GT by requiring that the imaginary part of the wave packet equals its real part. Other choices could have been made, but this one turns out to simplify the computations. The characteristics of each wave-packets α_i can finally be summarized as:

$$\begin{cases} \Re\left[\sigma_{\alpha_i}\right] &= f(0)\,\omega'_f(\mathbf{x}_i)/2, \\ \Im\left[\sigma_{\alpha_i}\right] &= \Re\left[\sigma_{\alpha_i}\right], \\ q_{\alpha_i}/p_{\alpha_i} &= -u'_f(\mathbf{x}_i)/v'_f(\mathbf{x}_i), \\ p_i &= \frac{\omega'_f(\mathbf{x}_i)\left(q_{\alpha_i}/p_{\alpha_i}\right)^2}{v'_f(\mathbf{x}_i)(1+\left(q_{\alpha_i}/p_{\alpha_i}\right)^2)}, \\ \mathbf{x}_{\alpha_i} &= \mathbf{x}_i. \end{cases} \tag{30}$$

This procedure creates N^2 wave-packets, from any vorticity field on a grid of size $2\pi/N$ and can be used to initialize the subgrid scale vorticity field from any given initial condition or to GT the force F by transforming it into an equivalent vorticity field $\omega'_f(\mathbf{x},t) = F(\mathbf{x},t)/dt$.

3.5 The Lagrangian scheme

A Lagrangian interpretation of the subgrid scale equation (15) shows that its time integration is equivalent to the evolution of each wave-packet in the ($\mathbf{x}$,$\mathbf{k}$) space. Each wave-packet carries a complex amount of Gabor vorticity (σ_α) and is advected at the resolved-scale velocity $\mathbf{U}(\mathbf{x})$, while its wavenumber and amplitude evolve according to the local resolved strain. For the trajectory of the wave-packet and its amplitude we have

$$\dot{\mathbf{x}}_\alpha = \mathbf{U}(\mathbf{x}_\alpha(t)), \tag{31}$$

$$\dot{\mathbf{k}}_\alpha = -\nabla_x \left(\mathbf{k}_\alpha(t) \cdot \mathbf{U}(\mathbf{x}_\alpha(t))\right), \quad (32)$$

$$\dot{\sigma}_\alpha = \hat{F}(\mathbf{x}_\alpha, \mathbf{k}_\alpha, t) - \nu_t k_\alpha^2 \sigma_\alpha. \quad (33)$$

By these equations, the wave-packets evolve continuously in the physical space in between the grid points associated with the finite, resolved-scale resolution. To find the resolved-scale quantities at the position of each particle (i.e. possibly in between grid mesh points), an interpolation procedure is used via the functions $S_{\mathbf{x}}$ and $S_{\mathbf{k}}$ associated with the PIC method.

3.6 Initial conditions

All the simulations used the same initial random vorticity field with all the energy concentrated at very large scales (the initial energy spectrum is given by $E(k) = ke^{-(k-k_o)^2}$ with $k_o = 1$). In practise, the noise associated with the PIC method is a function of the number of wave-packets used for computation. If the initial condition is such that the initial grid on which the vorticity is defined is too coarse (M too small), one can use a two step procedure to reach a reasonable number of wave-packets: in a first stage of the simulation, we create at each time step M^2 wave-packets with the vorticity $\omega'_f(\mathbf{x}, t) = F(\mathbf{x}, t)/dt$ created by the forcing F. During this stage, the wave-packets which were created at earlier times are moved into the phase space using the ray equations (31,32), but their amplitude is kept constant. This procedure is used until the total number of wave-packet reaches a desired number. From this point on, the wave-packet creation is shut down, and the wave-packets are evolved according to (31,32,33).

3.7 Noise reduction and effective turbulent viscosity

For inviscid simulations (when the turbulent viscosity is taken equal to 0), the numerical procedure develops a noise at very subgrid scales, which is a function both of the integration time and the total number of particles. We have found that an efficient way to reduce this subgrid-scale noise could be achieved by periodically recreating a new set of N_p wave-packets via first a rebuilding of the vorticity field in the physical space, on a grid of size $\sqrt{N_p}$ using (11), followed by a re-creation of wave-packets using (30). This procedure keeps the correlations associated with the subgrid-scale field unchanged, and therefore does not affect directly the resolved scale. In effect, this procedure acts as a filter for the subgrid scales which are smaller than the size of the reconstruction grid, and thus, can be seen as an effective

turbulent viscosity, which cannot be estimated a priori but which adjusts itself to the noise level.

3.8 Test of the accuracy of the method

To test the accuracy of our numerical method, we have performed *a priori* tests using data from a DNS at high resolution. The total vorticity field was divided into a subgrid-and a resolved-scale field using the same filter than in our model. The subgrid-scale field is further discretized into wave-packets according to eq. (30). A comparison was then made between the various components of the stresses in the DNS, and in our discretization scheme. The result of is shown fig. 4, which shows the square modulus of each of the three Reynolds stress components with respect to their wavenumbers. The accuracy of the discretized reconstruction of each terms is remarkable for the large scales. At very small scales ($k > 42$), the discretization tends to produce a noise in the components of the Reynolds stress involving the subgrid-scale velocity. In our case, we do not consider these terms so that we do not have to bother about this noise. In situations where one, or two of these troublesome terms are considered, the noise can be removed via a filtering at small scale. In spectral simulations, this truncature is provided naturally via the procedure to remove aliasing, which filters out modes larger than $2k_{max}/3$ where k_{max} is the maximum wavenumber of the resolved-scale field. The inset of figure 4 shows the comparison between the total real Reynolds stresses versus the total modeled Reynolds stress after desaliasing. The agreement is nearly perfect.

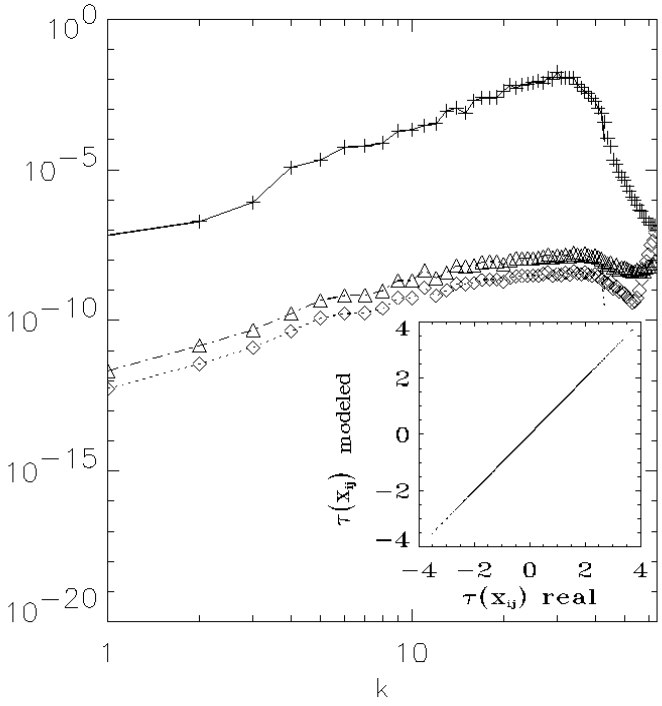

Figure 4: Moduli of the 3 non-linear terms in the resolved-scale equation (6) computed directly by the spectral method (lines) compared with the same fields rebuilt by the PIC method (symbols). Here, + and —— are used for the field $|\mathrm{div}\,\overline{(\mathbf{U}\omega')}(k)|^2$, $\triangle$ and $-\cdot-$ for $|\mathrm{div}\,\overline{(\mathbf{u}'\omega')}(k)|^2$ and $\diamond$ and $---$ for $|\mathrm{div}\,\overline{(\mathbf{u}'\Omega)}(k)|^2$). Corresponding comparison of the true and the PIC-modeled Reynolds Stresses $\tau = \mathrm{div}\,(\overline{\mathbf{u}\omega}) - \mathrm{div}\,(\overline{\mathbf{U}\Omega})$ at each grid point X_{ij} is shown in insert.

4 Numerical results

Our method can be used to perform two kind of simulations, depending on whether one is interested in the small-scale behavior or not. In the first case, one needs to model the subgrid scales with a large number of wave-packets, so as to be able to reconstruct the small-scale field with a good accuracy. Typically, one needs about $N_p = N^2$ wave-packets to be able to reconstruct faithfully details at scale $2\pi/N$ and to produce a result which may be compared with a Direct Numerical Simulation at resolution N^2. In the case when only large scales matter, one needs to keep the smallest number of wave-packet necessary to compute accurately the Reynolds stresses at the wavenumber cut-off. Since the resolved- scale field at the cut-off $k_c = M/2$ produces (by non-linear beating) information up to scale $2\pi/M$, we used a minimum of $N_p = M^2$ wave-packets in our "Large Eddy Simulations". Finally, note that our method allows nearly inviscid computations, since it does not require the existence of a viscosity at large scale and since it uses a minimal "effective viscosity" which starts acting only at scales $2\pi/M$. Very large Reynolds number can then be achieved via an adequate number of wave-packets.

We present results illustrating these points in two classical situations, - decaying and forced turbulence. In each case, the performance of our model are discussed and compared with results from the DNS and other popular subgrid-scale parameterizations used in 2D turbulence.

4.1 Decaying turbulence

For the decaying case, the initial condition was chosen so that the energy is concentrated at very large scales. The reference DNS was performed at a resolution $N^2 = 1024^2$ with a viscosity $\nu = 1.8\ 10^{-4}$, leading to a Reynolds number $Re \sim 10^4$. The simulation was stopped after approximatively 50 turnover times, by which time the initial condition has evolved into a robust dipole structure. The separation between resolved and subgrid scale used for our model is taken at $k_c = 21$, corresponding to a computation over a grid 64^2.

Let us first compare the DNS to our model using a large number of wave-packets ($N_p = 512^2$). We ran two different simulations: one in which the viscosity at resolved scale was set to $\nu = 1.8\ 10^{-4}$, like in the DNS ("viscous" simulation); another one in which ν was set to zero at resolved scale ("inviscid" simulation). The total simulation time of each simulation

is about 1h30 on a Sun workstation, roughly 150 times less than the DNS.

The total vorticity field after 50 turn over times, reconstructed by adding the contribution from the resolved and subgrid scales, is shown in Fig. 5 and compared with the vorticity field of the DNS. A global comparison for small and large scales can also be done via energy spectra. This is done in Fig. 6.

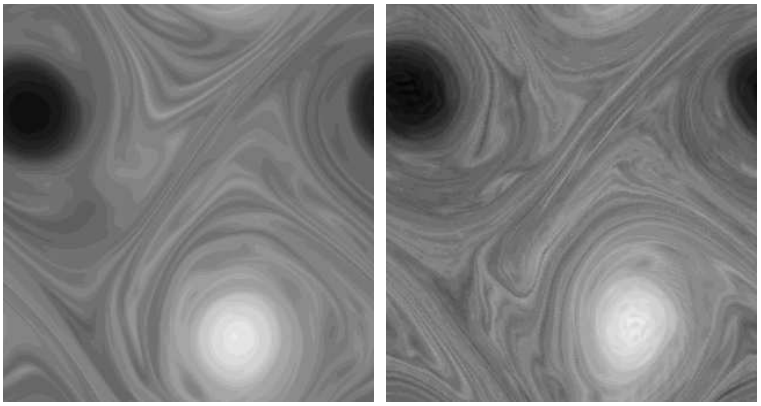

Figure 5: Total vorticity field of decaying turbulence after 50 turnover times as computed by DNS on a 1024^2 grid with viscosity $\nu = 1.8\ 10^{-4}$ (left) compared with the same field computed by the model M0 described in table 2 (right).

Clearly, the two pictures display good overall similarities at large scales, and marked differences at smaller scales. The largest structures are very similar and they are well localized even after 50 turnover times. The spectra in the two simulations overlap. The viscous simulation gives large-scale structures which are in closer agreement with the (viscous) DNS (see Table 2). Together, these results confirm that at large scale, the dynamically important coupling term between resolved and subgrid scale is the term $div(\overline{U}\omega')$, in agreement with the dynamical analysis of Laval et al [11], performed using a cut-off filter. At smaller scales, our model seems to produce thinner filaments and smaller structures. This effect is clearly visible on the spectra of the two simulations: in the DNS, the k^{-3} inertial law starts to level off towards $k = 60$ (due to viscous effects), while in our model, the power law extends over a wider range of scales, up to approximately $k = 100$. To check whether this difference comes from our subgrid scale scheme, we performed a direct comparison of the smallest scales of the simulation $k > 21$. Fig.

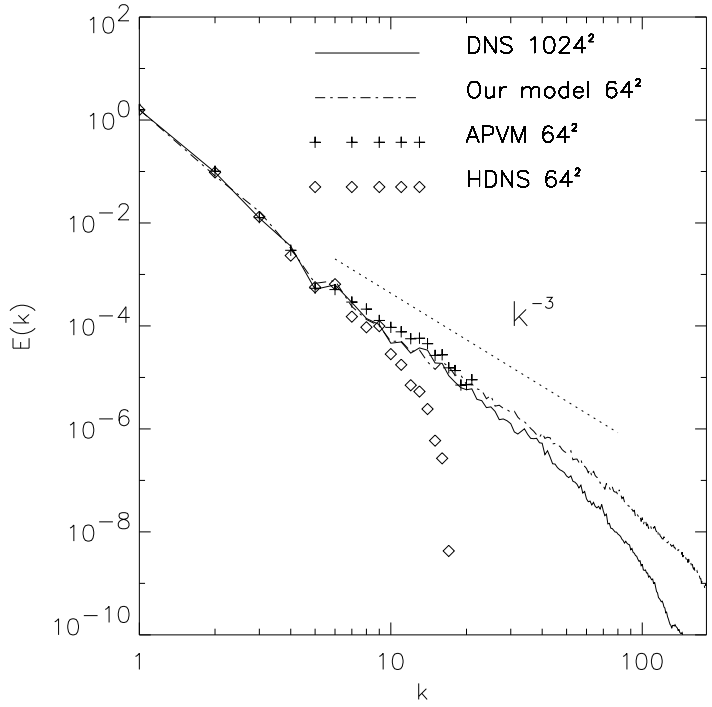

Figure 6: The energy spectra obtained by the same simulation as in fig. 2 compared with the spectra obtained by some other methods including our model with parameters M0 from the table 2.

7 shows such a comparison at some earlier time (after about 15 turnover times), when the small scales have not yet been washed out by viscosity. At this time, differences are negligible, proving that our model also captures the dominant coupling mechanism at subgrid scales. This finding is also in agreement with the dynamical analysis of Laval et al [11]. The further differences arising over longer time scales can therefore be due to two effects: one is the error accumulation due to sub-dominant neglected terms in our model (like the terms involving coupling of the resolved vorticity Ω with the subgrid velocity $\mathbf{u}'$); the second is viscous effects. We believe that the first possibility is ruled out by the dynamical analysis of Laval et al [11], in which numerical simulations of our model equations were performed us-

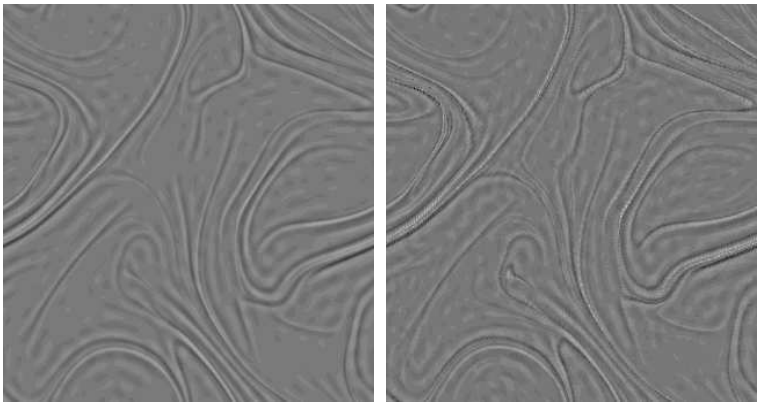

Figure 7: Small-Scale vorticity field of decaying turbulence after 15 turnovers. Result from a DNS on a 1024^2 grid with $\nu = 1.8\ 10^{-4}$ (left) and from our model (M0).

ing the same viscosity than in the direct numerical simulations [2]. In that case, the differences at small scales appear to be negligible. We therefore interpret the differences between the two models as a viscous effect, and, actually, as an indication of the lower effective viscosity in our model. This would explain both the later bending of the spectra, and the finer structure of the filaments.

The second series of comparison were performed using the minimum number of wave-packet, equal in the present case to $N_p = 128^2$. In such a case, the number of wave-packets does not allow accurate reconstruction for the scales less than $2\pi/128$. The simulation is however much faster, and takes only 8 minutes of computational time. The total large-scale vorticity field after 50 turn over times is compared with the corresponding large-scale vorticity field of the DNS in Fig. 8. The agreement is still very good and to quantify this agreement, we computed the correlation coefficient between the two simulations, defined by:

$$C_{1,2} = \frac{\sum_{1<i,j<64} \omega_1(i,j)\omega_2(i,j)}{\sqrt{\sum_{1<i,j<64} \omega_1(i,j)^2 \sum_{1<i,j<64} \omega_1(i,j)^2}} \tag{34}$$

where $\omega_1(i,j)$ and $\omega_2(i,j)$ are the large-scale vorticity field. This correlation coefficient was computed at two different times, corresponding to 15

[2] These simulations were not fast: they were based on spectral methods and were even more slowly than the direct method.

and 50 turnover time, and reported in table 2. At earlier time, our three models (viscous or not) are all characterized by a very good correlation coefficient (about 99 percent). At later time, a slight difference appear. In fact, the best correlations are achieved by the viscous model, and the model with the least number of subgrid-scale modes. This is not surprising, since our noise removing procedure produces an effective viscosity which is larger as the number of subgrid-scale modes decreases. The high resolution model M1 is then the less viscous model of all three, and therefore, can be expected to produces the largest difference with respect to the viscous DNS.

Two other popular 2D turbulent model were also tested along the same line. In the first one (HDNS), the viscous term $\nu\Delta\Omega$ of the Navier-Stokes equation is replaced by a "hyper-viscous" term $\nu_p\Delta^p\Omega$. In our simulations, we took $p = 8$ and $\nu_p = 10^{-18}$. The second model is the Anticipated Potential Vorticity Model (APVM) developed by Sadourny and Basdevant [23]. Both models are very cheap, taking only about 2 minutes of computational time. They are also less accurate, as can be seen from both the Fig. 8, and the table. In the HDNS 64^2, the correlation coefficient is only about 50 percent in the end of the simulation. For the APVM, it is higher (about 75 percent), but still lower than our "minimal model". The energy spectra of the 4 simulations can also be compared. This is done in Fig. 6. Our model develops an energy spectrum very close to the APVM one, and slightly less steep than the DNS at scales close to the cut-off. This is because at this scale, viscous effects start being felt and tend to bend the spectrum. The HDNS spectrum is much steeper near the cut-off than both the reference DNS and the two other models.

4.2 Forced turbulence

Similar simulations were performed in the case of forced turbulence. In such a case, our model was ran with $M^2 = 64^2$ resolved-scale Fourier modes, and $N_p = 512^2$ subgrid-scale Gabor modes, and no additional viscosity. Run were also performed using a HDNS or the APVM model over 64^2 Fourier modes. The initial condition is a vorticity field with an energy spectrum concentrated at the forced wavenumber (k=15) and with a small amount of total energy. The simulation was forced by keeping constant the energy of the mode $\mathbf{k}$=(15,0). In this situation, the vorticity field is progressively built via the stochastic forcing, which is itself strongly dependent on the exact structure of the vorticity field (since it must aim at keeping one mode constant). Due to the developing spectral cascades, the scale interactions

become less nonlocal and we may then expect sub-dominant terms to play an enhanced role (with respect to the decaying case). Indeed, we have observed that the vorticity fields in the DNS and in the model do not exactly correspond: both simulations display similar small scale intense vortices, but they are not located at the same places. This effect can also be seen more clearly in the spectra. They are shown in fig. 9. Due to the chaoticity, they all differ at the mode $k = 1$ which is the most sensitive to the exact position of each individual vortex. At smaller scales, marked differences appear between the models. Clearly, the HDNS gives the worst result, with a large deficit of energy over all scales. This is because in this case, the forcing scale is very close to the scale at which the dissipation takes place, and most of the energy is dissipated before the inverse cascade to larger scales can occur. The two other models, which do not introduce an explicit dissipation at the cut-off scale, perform much better. The APVM model tends to overestimate the rate of energy at the largest scale and to underestimate it in the inertial range. Our model slightly underestimates the amount of energy at the largest scale, but gives results very close to the DNS in the inertial range of scale. At scales smaller than the cut-off, both the DNS and our model produce an energy spectra steeper than the k^{-3} law. At the largest wavenumber, the beginning of the viscous range is clearly visible in the DNS but not in our model. This is again an indication of the large Reynolds number achieved by our model. As for computational times, the performances are similar to the decaying case.

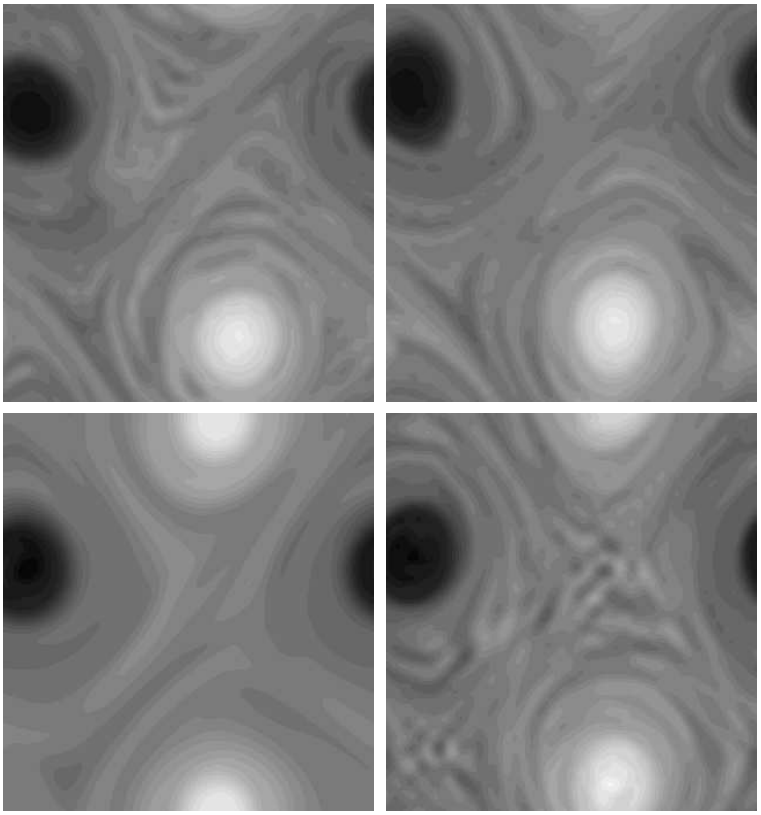

Figure 8: Large-scale vorticity field ($k \leq 21$) after 50 turnover times in decaying turbulence. **upper left**: DNS on a 1024^2 grid and $\nu = 1.8\ 10^{-4}$, **upper right**: our model (M2 in table 2) with a separation scale at $k = 21$ and 16384 modes in subgrid scales, **lower left**: simulation with hyper-viscosity (using $\nu_p k^p \omega$ as the dissipation term with p=8) on a 64^2 grid and **lower right**: simulation with the APVM model ([23]) on a 64^2 grid.

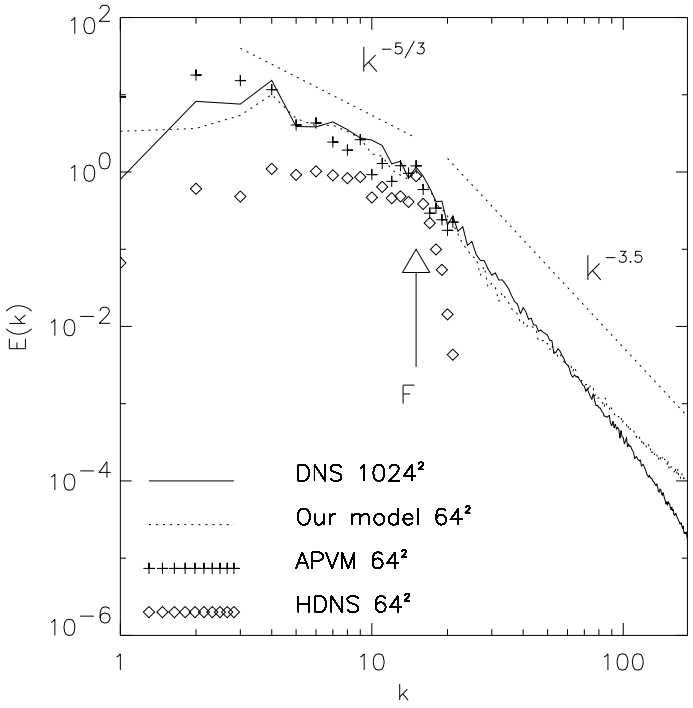

Figure 9: Comparison of the energy spectra of forced turbulence after 150 turnover times computed by different methods (our model refers to the run M0 from the table 2)

5 Discussion

We developed a new dynamic model of subgrid-scale turbulence based on a simple hypothesis about the subgrid-scale evolution. This approach is different from traditional turbulent models since our model provides expressions of the turbulent Reynolds sub-grid stresses via estimates of the sub-grid velocities rather than velocities correlations. The subgrid-scale dynamic is given by a linear equation, describing the advection of subgrid-scale wave-packets with the mean flow. This feature allows a reduction of the time step used in the simulation, via the use of a pseudo-Lagrangian method. We thereby achieved a reduction of the computational time by a factor 150 in the typical cases we considered. Our method can also be used for Large Eddy Simulation strategies, in which only the large scales are computed. This allows a large memory savings, and an additional reduction of the computational time (typically a factor 10 in the case we considered). The resulting simulation is more costly than a traditional LES simulation, based on Fast Fourier Transform algorithms (like hyperviscosity or vorticity dissipative schemes). It could however become more competitive for more complicated geometries, where finite difference schemes become more appropriate than FFT. This would make LES models based on hyperviscous schemes much more costly, while our method would proportionally keep at the same computational performance.

In the present paper, only 2D turbulence has been considered. As is well known, 2D turbulence is very special, because there is no vortex stretching. One may therefore wonder whether our model could be applied to 3D flows. To answer this question, Laval and Dubrulle [12] have recently performed a numerical analysis of the hypotheses pertaining our turbulent model. The main hypothesis is that the subgrid dynamics can be very well approximated by an equation in which non-local terms are retained, while local terms (non-linear in the subgrid velocities) are replaced by a turbulent viscosity. The numerical analysis, performed via a numerical simulation of the coupled resolved and approximate subgrid equations indeed showed that such hypothesis is valid, insofar as both the energy spectra, the structures and the statistical properties of such a model were very close to that of a DNS. Even so this analysis can only be performed at a rather moderate Reynolds number (80 to 200, based on the Taylor scale), we find this analysis encouraging.

A Derivation of the subgrid scale equation in (x,k) space

Some properties of the GT will be useful in the sequel. They are (see [13, 15] for details):

$$\begin{aligned} \widehat{\partial_i \mathbf{u}'}(\mathbf{x},\mathbf{k},t) &= \partial_i \hat{\mathbf{u}}'(\mathbf{x},\mathbf{k},t) && (35)\\ &= ik_i \hat{\mathbf{u}}'(\mathbf{x},\mathbf{k},t) + O(\epsilon^*) && (36) \end{aligned}$$

$$\widehat{\mathbf{U}\omega'}(\mathbf{x},\mathbf{k},t) \simeq \mathbf{U}(\mathbf{x},t)\hat{\omega}'(\mathbf{x},\mathbf{k},t) + i\ (\nabla_x \cdot \nabla_k)\,\mathbf{U}\omega'. \quad (37)$$

Let us derive the GT of the equation:

$$\partial_t \omega' + div(U_j \omega') = F(\mathbf{x},t) + \nu_t \Delta \omega'. \quad (38)$$

Using (36), we find that the GT of the viscous term is $-\nu_t k^2 \hat{\omega}'$. The GT and the time derivative commute, so that the GT of the first term of the lhs gives :

$$\widehat{\partial_t \omega'} = \partial_t\ \hat{\omega}' \quad (39)$$

Using the space derivative property (36), the GT of the second terms can be developed into:

$$\begin{aligned} \widehat{\partial_j U_j \omega'} &= \widehat{U_j \partial_j \omega'} && (40)\\ &\simeq U_j\ \widehat{\partial_j \omega'} + i\,\partial_l U_j \frac{\partial}{\partial k_l} \widehat{\partial_j \omega'} \\ &\simeq U_j \partial_j \hat{\omega}' + i\,\partial_l U_j \frac{\partial}{\partial k_l}\left(i k_j \hat{\omega}'\right) \\ &\simeq U_j \partial_j \hat{\omega}' + i\,\partial_l U_j k_j \frac{\partial}{\partial k_l}\hat{\omega}' - \hat{\omega}' \partial_j U_j \end{aligned}$$

Using the incompressibility ($\partial_j U_j = 0$), we finally obtain :

$$D_t\,\hat{\omega}'(\mathbf{x},\mathbf{k},t) = \hat{F}(\mathbf{x},t) - \nu_t k^2 \hat{\omega}'(\mathbf{x},\mathbf{k},t) \quad (41)$$

with :

$$\begin{aligned} D_t &= \partial_t + \mathbf{U}\cdot\nabla - \nabla_x\,(\mathbf{U}\cdot\mathbf{k})\cdot\nabla_k, && (42)\\ & && (43) \end{aligned}$$

B Reconstruction formulae for the correlations

Using the formula 36 for the GT of space derivative, one can derive the subgrid scale velocity field in the (**x**,**k**) space with respect to the subgrid scale vorticity:

$$\begin{aligned}\hat{\omega'}(x,y,p,q,t) &= \widehat{\partial_x v'}(x,y,p,q,t) - \widehat{\partial_y u'}(x,y,p,q,t) \\ &= \partial_x \hat{v'}(x,y,p,q,t) - \partial_y \hat{u'}(x,y,p,q,t) \\ &= i\,p\,\hat{v'}(x,y,p,q,t) - i\,q\,\hat{u'}(x,y,p,q,t) + O(\epsilon^\star),\end{aligned} \tag{44}$$

where $\mathbf{k} = (p,q)$ and $\mathbf{x} = (x,y)$. Reversing the formula, we obtain the expression of the Gabor Transform of the velocity:

$$\hat{u'}(x,y,p,q,t) = \frac{iq}{p^2+q^2}\,\hat{\omega'}(x,y,p,q,t) + O(\epsilon^\star), \tag{45}$$

$$\hat{v'}(x,y,p,q,t) = \frac{-ip}{p^2+q^2}\,\hat{\omega'}(x,y,p,q,t) + O(\epsilon^\star). \tag{46}$$

Consider now the following expression:

$$\begin{aligned}&\int \frac{1}{2}\left[\hat{u'}(\mathbf{x},\mathbf{k},t)\hat{\omega'}(\mathbf{x},-\mathbf{k},t) + \hat{u'}(\mathbf{x},-\mathbf{k},t)\hat{\omega'}(\mathbf{x},\mathbf{k},t)\right] d\mathbf{k} \\ =\ &\int \Re\left[\hat{u'}(\mathbf{x},\mathbf{k},t)\hat{\omega'}(\mathbf{x},-\mathbf{k},t)\right] d\mathbf{k} \\ =\ &\int \Re\left[\int f(\epsilon^\star(\mathbf{x}-\mathbf{x}'))e^{i\mathbf{k}(\mathbf{x}-\mathbf{x}')}u'(\mathbf{x}',t)d\mathbf{x}' \int f(\epsilon^\star(\mathbf{x}-\mathbf{x}''))e^{i\mathbf{k}(\mathbf{x}-\mathbf{x}'')}\omega'(\mathbf{x}'',t)d\mathbf{x}''\right] d\mathbf{k} \\ =\ &\int f(\epsilon^\star(\mathbf{x}-\mathbf{x}'))f(\epsilon^\star(\mathbf{x}-\mathbf{x}''))u'(\mathbf{x}',t)\omega'(\mathbf{x}'',t)\left(\int e^{i\mathbf{k}(\mathbf{x}''-\mathbf{x}')}d\mathbf{k}\right) d\mathbf{x}'d\mathbf{x}''.\end{aligned} \tag{47}$$

Using the definition of the Dirac function,

$$\frac{1}{(2\pi)^2}\int e^{i\mathbf{k}(\mathbf{x}''-\mathbf{x}')}d\mathbf{k} = \delta(\mathbf{x}'-\mathbf{x}''), \tag{48}$$

and the fact that $f^2 = G$, one simply gets

$$\frac{1}{(2\pi)^2}\int \Re\left[\hat{u'}(\mathbf{x},\mathbf{k},t)\hat{\omega'}(\mathbf{x},-\mathbf{k},t)\right] d\mathbf{k} = \overline{u'\omega'}(\mathbf{x},t). \tag{49}$$

We may proceed along the same line for the average of the non-linear product of a large scale field with a subgrid scale field. Using the definition of the average $\overline{\mathbf{U}\omega'}(\mathbf{x},t)$ can be written as follows,

$$\overline{\mathbf{U}\omega'}(\mathbf{x},t) = \int f^2(\epsilon^\star(\mathbf{x}-\mathbf{x}'))\mathbf{U}(\mathbf{x}',t)\omega'(\mathbf{x}',t)d\mathbf{x}'. \tag{50}$$

Using the Taylor development of U with respect to $\mathbf{x}$ at the first order, we obtain the first order approximation of this term:

$$\begin{aligned}\overline{\mathbf{U}\omega'}(\mathbf{x},t) &= (\mathbf{U}\overline{\omega'})(\mathbf{x}) + \int f^2(\epsilon^\star(\mathbf{x}-\mathbf{x}'))(\mathbf{x}-\mathbf{x}')\nabla\mathbf{U}(\mathbf{x}',t)\omega'(\mathbf{x}',t)d\mathbf{x}' \\ &= (\mathbf{U}\overline{\omega'})(\mathbf{x}) + O(\epsilon^\star). \end{aligned} \tag{51}$$

If we now apply the definition of the average for a product of two subgrid scales field (49) with the quantities 1 et ω', we finally obtain:

$$\overline{\mathbf{U}\omega'}(\mathbf{x},t) = \mathbf{U}\frac{1}{(2\pi)^2}\int \Re\left[\hat{\omega'}(\mathbf{x},\mathbf{k},t)\hat{1}(\mathbf{x},-\mathbf{k},t)\right]d\mathbf{k} + O(\epsilon^\star) \tag{52}$$

$$= \mathbf{U}\frac{1}{(2\pi)^2}\int \Re\left[\hat{\omega'}(\mathbf{x},\mathbf{k},t)\hat{f}(k)\right]d\mathbf{k} + O(\epsilon^\star). \tag{53}$$

C Numerical computation of the Reynolds Stress components

The subgrid scale field in physical space can be obtained from their discrete formula in the ($\mathbf{x}$,$\mathbf{k}$) by an integration with respect to $\mathbf{k}$:

$$\begin{aligned}\omega'(\mathbf{x},t) &= \frac{1}{(2\pi)^2\, f(0)}\int \hat{\omega'}(\mathbf{x},\mathbf{k},t)d\mathbf{k} \qquad (54)\\ &= \frac{1}{(2\pi)^2\, f(0)}\int \sum_{\alpha=1}^{2N_p}\hat{\sigma}_\alpha(t)\; S_{\mathbf{x}}(\mathbf{x}-\mathbf{x}_\alpha(t))\; \delta(\mathbf{k}-\mathbf{k}_\alpha(t))\, d\mathbf{k} \\ &= \frac{1}{f(0)}\sum_{\alpha=1}^{2N_p}\hat{\sigma}_\alpha(t)\; S_{\mathbf{x}}(\mathbf{x}-\mathbf{x}_\alpha(t)) \\ &= \frac{1}{f(0)}\left\{\sum_{\alpha_+=1}^{N_p}\hat{\sigma}_{\alpha_+}(t)\; S_{\mathbf{x}}(\mathbf{x}-\mathbf{x}_{\alpha_+}(t)) + \sum_{\alpha_-=1}^{N_p}\hat{\sigma}_{\alpha_1}(t)\; S_{\mathbf{x}}(\mathbf{x}-\mathbf{x}_{\alpha_-}(t))\right\}, \end{aligned}$$

where

$$\sum_{\alpha=1}^{2N_p} = \sum_{\alpha_+=1}^{N_p} + \sum_{\alpha_-=1}^{N_p}, \tag{55}$$

$\sum_{\alpha_+=1}^{N_p}$ means sum over half the particles with the wavenumber $\mathbf{k}_\alpha$ and $\sum_{\alpha_-=1}^{N_p}$ is the sum over particles with an opposite wavenumber $-\mathbf{k}_\alpha$. We

choose the "positive" particles α_+ with $p_{\alpha_+} > 0$ and $\mathbf{k}_\alpha = (p_{\alpha_+}, q_{\alpha_+})$. Because $\mathbf{x}_{\alpha_+} = \mathbf{x}_{\alpha_-}$, $\omega'(\mathbf{x}, t)$ can be written:

$$\omega'(\mathbf{x}, t) = \frac{1}{f(0)} \sum_{\alpha_+=1}^{N_p} \left(\hat{\sigma}_{\alpha_+}(t) + \hat{\sigma}_{\alpha_-}(t)\right) S_{\mathbf{x}}(\mathbf{x} - \mathbf{x}_{\alpha_+}(t)). \tag{56}$$

Since $\omega'(\mathbf{x}, t)$ is real, the following property holds:

$$\hat{\sigma}_{\alpha_+}(t) = \hat{\sigma}^*_{\alpha_-}(t) \tag{57}$$

and the formula used to rebuild the vorticity field in physical space is :

$$\omega'(\mathbf{x}, t) = \frac{2}{f(0)} \sum_{\alpha_+=1}^{N_p} \Re\left[\hat{\sigma}_{\alpha_+}(t)\right] \; S_{\mathbf{x}}(\mathbf{x} - \mathbf{x}_{\alpha_+}(t)) \tag{58}$$

where $\Re\left[\hat{\sigma}_{\alpha_+}(t)\right]$ is the real part of $\hat{\sigma}_{\alpha_+}(t)$. The same developments can be made for the two velocity component, using (45) and (46):

$$u'(\mathbf{x}, t) = \frac{2}{f(0)} \sum_{\alpha_+=1}^{N_p} \frac{-q_{\alpha_+}}{{p_{\alpha_+}}^2 + {q_{\alpha_+}}^2} \Im\left[\hat{\sigma}_{\alpha_+}(t)\right] \; S_{\mathbf{x}}(\mathbf{x} - \mathbf{x}_{\alpha_+}(t)) \tag{59}$$

$$v'(\mathbf{x}, t) = \frac{2}{f(0)} \sum_{\alpha_+=1}^{N_p} \frac{p_{\alpha_+}}{{p_{\alpha_+}}^2 + {q_{\alpha_+}}^2} \Im\left[\hat{\sigma}_{\alpha_+}(t)\right] \; S_{\mathbf{x}}(\mathbf{x} - \mathbf{x}_{\alpha_+}(t)) \tag{60}$$

where $\Im\left[\hat{\sigma}_{\alpha_+}(t)\right]$ is now the Imaginary part of $\hat{\sigma}_{\alpha_+}(t)$.

The previous expressions can be used to compute velocity correlations. Using the analytical definition of these terms with respect the the subgrid scales field in ($\mathbf{x}$,$\mathbf{k}$) space (49,53), and using the definition of the subgrid scale discretization (16), we get:

$$\begin{aligned}
\overline{u'v'}(\mathbf{x}, t) &= \frac{1}{(2\pi)^2} \int \Re\left[\hat{u'}(\mathbf{x}, \mathbf{k}, t)\hat{v'}(\mathbf{x}, -\mathbf{k}, t)\right] d\mathbf{k} \qquad (61)\\
&= \frac{1}{(2\pi)^2} \int \Re\left[\left(\sum_{\alpha=1}^{2N_p} \frac{iq}{p^2+q^2}\, \hat{\sigma}_\alpha\, S_{\mathbf{x}}(\mathbf{x} - \mathbf{x}_\alpha)\delta(\mathbf{k} - \mathbf{k}_\alpha)\right)\right.\\
&\qquad \left.\left(\sum_{\beta=1}^{2N_p} \frac{+ip}{p^2+q^2}\, \hat{\sigma}_\beta\, S_{\mathbf{x}}(\mathbf{x} - \mathbf{x}_\beta)\delta(-\mathbf{k} - \mathbf{k}_\beta)\right)\right] d\mathbf{k}.
\end{aligned}$$

If all the wave-packets have a different wavenumber (at least on a domain equal to the "support" of S_x), eq 62 can be written:

$$\overline{u'v'}(\mathbf{x},t) = 2\sum_{\alpha_+=1}^{N_p} \Re\left[\frac{-q_{\alpha_+}p_{\alpha_+}}{({p_{\alpha_+}}^2+{q_{\alpha_+}}^2)^2}\hat{\sigma}_{\alpha_+}\hat{\sigma}_{\alpha_-}S^2_{\mathbf{x}}(\mathbf{x}-\mathbf{x}_{\alpha_+})\right]. \tag{62}$$

Using the fact that $\hat{\sigma}_{\alpha_-}$ and $\hat{\sigma}_{\alpha_+}$ are complex conjugate, we finally get:

$$\begin{aligned}
\overline{u'v'}(\mathbf{x},t) &= 2\sum_{\alpha_+=1}^{N_p} \frac{-q_{\alpha_+}p_{\alpha_+}}{({p_{\alpha_+}}^2+{q_{\alpha_+}}^2)^2}|\hat{\sigma}_{\alpha_+}|^2 S^2_{\mathbf{x}}(\mathbf{x}-\mathbf{x}_{\alpha_+}),\\
\overline{u'^2}(\mathbf{x},t) &= 2\sum_{\alpha_+=1}^{N_p} \frac{+q^2_{\alpha_+}}{({p_{\alpha_+}}^2+{q_{\alpha_+}}^2)^2}|\hat{\sigma}_{\alpha_+}|^2 S^2_{\mathbf{x}}(\mathbf{x}-\mathbf{x}_{\alpha_+}),\\
\overline{v'^2}(\mathbf{x},t) &= 2\sum_{\alpha_+=1}^{N_p} \frac{+p^2_{\alpha_+}}{({p_{\alpha_+}}^2+{q_{\alpha_+}}^2)^2}|\hat{\sigma}_{\alpha_+}|^2 S^2_{\mathbf{x}}(\mathbf{x}-\mathbf{x}_{\alpha_+}).
\end{aligned} \tag{63}$$

The non-linear term involving the resolved scale velocity field can also be written in terms of wave-packets coordinates. Using eq. (53) and the definition of discretization (16) , one can write:

$$\begin{aligned}
\overline{\mathbf{U}\omega'}(\mathbf{x},t) &\simeq \frac{\mathbf{U}}{(2\pi)^2}\int \Re\left[\hat{\omega'}(\mathbf{x},\mathbf{k},t)\hat{1}(\mathbf{x},-\mathbf{k},t)\right]d\mathbf{k}\\
&\simeq \frac{\mathbf{U}}{(2\pi)^2}\int \Re\left[\hat{\omega'}(\mathbf{x},\mathbf{k},t)f(-\mathbf{k})\right]d\mathbf{k}\\
&\simeq \frac{\mathbf{U}}{(2\pi)^2}\int \Re\left[\sum_{\alpha=1}^{2N_p}\hat{\sigma_\alpha}f^*(\mathbf{k})S_{\mathbf{x}}(\mathbf{x}-\mathbf{x}_\alpha)\delta(\mathbf{k}-\mathbf{k}_\alpha)\right]d\mathbf{k}\\
&\simeq 2\mathbf{U}\sum_{\alpha_+=1}^{N_p}\Re\left[\hat{\sigma_{\alpha_+}}f^*(\mathbf{k}_{\alpha_+})\right]S_{\mathbf{x}}(\mathbf{x}-\mathbf{x}_{\alpha_+}).
\end{aligned} \tag{64}$$

D Choice of the filter

The choice of the interpolating function $S_x(\mathbf{x})$ (eq. 17) dictates the shape of the filter and, therefore, of the unknown function $f(x)$ in the definition of the Gabor Transform. The proof proceeds via the quantity $\overline{\omega'^2}(\mathbf{x},t)$, by equating the formula of the filter discretized on a regular grid with a cell

size $\Delta\mathbf{x}$ and the formula 58:

$$\overline{\omega'^2}(\mathbf{x},t) = \sum_i \omega'^2(\mathbf{x}_i)\, f^2(\mathbf{x}-\mathbf{x}_i)\,(\Delta\mathbf{x})^2 \quad (65)$$

$$= 2\sum_{\alpha_+=1}^{N_p} |\sigma_{\alpha_+}|^2\, S^2_{\mathbf{x}}(\mathbf{x}-\mathbf{x}_{\alpha_+}) \quad (66)$$

For this equality to be valid at all grid point X_i, the following link between f and S must hold:

$$f^2(\mathbf{x}) = C \times S^2_{\mathbf{x}}(\mathbf{x}). \quad (67)$$

Using now the normalization:

$$S_{\mathbf{x}}(0) = 1. \quad (68)$$

$$\int f^2(\mathbf{x}')d\mathbf{x}' = 1. \quad (69)$$

the eq. 67 becomes:

$$f(\mathbf{x}) = f(0)\, S_{\mathbf{x}}(\mathbf{x}) \quad (70)$$

with

$$f(0) = \frac{1}{\sqrt{\int S^2_{\mathbf{x}}(\mathbf{x}')d\mathbf{x}'}}. \quad (71)$$

References

[1] Leonard, A., *Direct numerical simulations, in turbulence and its simulation.* (T. Gatski, ed.), Springer, 1995.

[2] Werne, J. and D. C. Fritts, "Stratified shear turbulence: Evolution and statistics", *Geophys. Research Lett.*, vol. 26, 1999, pp. 439–442.

[3] Joslin, R. D. "Discussion of DNS: past, present and future". In *First international conference on direct numerical simulation and large eddy simulation (DNS/LES).* (Ruston, Louisiana, 1997).

[4] Grossmann, S., D. Lohse and A. Reech, "Developped turbulence: from full simulations to full mode reductions", *Phys. Rev. Lett.*, vol. 77, 1996, pp. 5369–5372.

[5] Meneguzzi, M., H. Politano, A. Pouquet and M. Zolver, "A sparse-mode spectral method for the simulation of turbulent flows", *J. of Computational Phys.*, vol. 123, 1996, pp. 32–44.

[6] Schneider, K., N. K.-R. Kevlahan and M. Farge, "Comparison of an adaptative wavelet method and nonlinearly filtered pseudospectral methods for two-dimensional turbulence.", *Theore. Comput. Fluid Dynamics*, vol. 9, 1997, pp. 191–206.

[7] Berger, M. J. and J. Oliger, "Adaptative mesh refinement for hyperbolic partial differential equations", *J. Comput. Phys.*, vol. 53, 1984, p. 484.

[8] Berger, M. J. and P. Collela, "Local adaptative mesh refinement for shock hydrodynamics", *J. Comput. Phys.*, vol. 82, 1989, p. 64.

[9] Oberlack, M. "Unified theory for symmetries in plane parallel turbulent shear flows". Tech. Rep. manuscript no. 163, under review in J. Fluid Mech., Center for Turbulence Research, Stanford University/NASA Ames, 1997.

[10] Laval, J.-P., B. Dubrulle and S. Nazarenko, "Dynamical modeling of sub-grid scales in 2D turbulence", *Physica D: Nonlinear Phenomena*, vol. 142, 2000, pp. 231–253.

[11] Laval, J.-P., B. Dubrulle and S. Nazarenko, "Nonlocality of interaction of scales in the dynamics of 2D incompressible fluids", *Phys. Rev. Lett.*, vol. 83, 1999, pp. 4061–4064.

[12] Laval, J.-P. and B Dubrulle, "Numerical validation of a dynamical turbulent model of turbulence", *submitted to Phys. Rev. Lett.*, 2000.

[13] Nazarenko, S., N. K.-R. Kevlahan and B. Dubrulle, "Nonlinear RDT theory of near-wall turbulence", *Physica D*, vol. 139, 2000, pp. 158–176.

[14] Nazarenko, S., N. K.-R. Kevlahan and B. Dubrulle, "Semiclassical theory for rapid distortion of homogeneous turbulence", *J. Fluid Mech.*, vol. 390, 1999, p. 325.

[15] Dubrulle, B., J.-P. Laval, S. V. Nazarenko and N. K.-R. Kevlahan, "Derivation of equilibrium profiles in plane parallel flows using a dynamic subgrid-scale model", *Submitted to Phys. Fluids*, 1999.

[16] Dubrulle, B., J.-P. Laval and P. Sullivan, "A new dynamical subgrid model for the planetary surface layer. I the model.", *submitted to J. Atmosph. Science.*, 1999.

[17] Dubrulle, B., J.-P. Laval and P. Sullivan, "A new dynamical subgrid model for the planetary surface layer. II analytical computation of fluxes, mean profiles and variances", *submitted to J. Atmosph. Science.*, 1999.

[18] Nazarenko, S. and J.-P. Laval, "Non-local 2D turbulence and Batchelor's regime for passive scalars", *J. Fluid Mech.*, vol. 408, 2000, pp. 301–321.

[19] Brachet, M. E., M. Meneguzzi, H. Politano and P. L. Sulem, "The dynamics of freely decaying two-dimensional turbulence", *J. Fluid Mech.*, vol. 194, 1988, pp. 333–349.

[20] Farge, M., N. K.-R. Kevlahan, V. Perrier and E. Goirand, "Wavelets and turbulence", *Proceeding of the IEEE*, vol. 84, 1996, pp. 639–669.

[21] Farge, M., K. Schneider and N. K.-R. Kevlahan, "Non-gaussianity and coherent vortex simulation for two-dimensional turbulence using an adaptadive orthogonal wavelet basis", *Phys. Fluids*, vol. 11, 1999, pp. 2187–2201.

[22] Nazarenko, S., N. Zabusky and T. Scheidegger, "Nonlinear sound-vortex interactions in an inviscid isentropic fluid: a two fluid model", *Phys. Fluid*, vol. 7, 1995, p. 2407.

[23] Sadourny, R. and C. Basdevant, "Parametrization of subgrid scale barotropic eddies in quasi-geotrophic models: Anticipated potential vorticity method", *J. Atm. Sci.*, vol. 42, 1985, pp. 1353–1363.